RSC Advances

PAPER

View Article Online
View Journal | View Issue

Cite this: *RSC Adv.*, 2026, **16**, 21655

Synthesis and antibacterial activity study of anti-biofilm agents based on American oyster defensin analog A4

Xin Zhang,† Yu Liu,† Zhixing Geng and Ye Guo *

Chronic infections caused by bacterial biofilms represent a challenging clinical issue. The formation of biofilms markedly complicates the treatment of bacterial infections and frequently contributes to the development of drug-resistant strains. Anti-biofilm agents, encompassing a class of chemically or biologically active substances, are capable of inhibiting the formation of microbial biofilms or disrupting pre-existing biofilm structures. Antimicrobial peptides, as anti-biofilm agents, effectively interfere with the formation and stability of biofilms. As an analog of American oyster defensin (AOD), A4 displays superior antibacterial activity, diverse modes of action (including DNA interaction and inhibition of DNA amplification), and low toxicity. The purpose of this study is to develop new anti-biofilm agents with higher activity and better stability based on A4. By tuning amino acid configuration and substituting disulfide bonds, four analogs (D-A4, A4-T1, A4-T2, and A4-T3) were designed and synthesized. Results of antibacterial assays indicated that all analogs maintained broad-spectrum antibacterial activity, with D-A4 exhibiting enhanced antibacterial efficacy. Crystal violet staining assays demonstrated that D-A4 effectively inhibited biofilm formation at concentrations as low as 1/2 × MIC. Stability assays revealed that D-A4 exhibited high stability in both proteolytic and serum environments. With potent activity, excellent stability, and low toxicity, D-A4 holds great promise as an anti-biofilm agent against multidrug-resistant bacterial infections.

Received 27th March 2026
Accepted 19th April 2026

DOI: 10.1039/d6ra02550a

rsc.li/rsc-advances

1 Introduction

Bacterial biofilms are structured microbial communities formed by bacterial adhesion to biotic or abiotic surfaces. In the field of global clinical anti-infective treatment, chronic infections arising from bacterial biofilms constitute a persistent and formidable challenge for healthcare practitioners.[1] The formation of biofilms substantially enhances the resistance of bacteria to antibiotics. Owing to the intricate protective mechanisms afforded by biofilms, the management of chronic infections often requires antibiotic dosages several orders of magnitude higher than standard therapeutic levels.[2] The administration of high-dose antibiotics not only increases the risk of toxicity and adverse effects but also promotes drug-resistant bacteria.[3] Current therapeutic strategies for managing bacterial biofilm-associated infections are constrained by challenges, including the emergence of antibacterial resistance and insufficient targeted specificity.[4,5] Consequently, the development of novel anti-biofilm agents that are not prone to developing drug resistance and are capable of inhibiting biofilm formation has become an urgent necessity in the current field of anti-infection research.

Antimicrobial peptides (AMPs) are fundamental components of the innate immune system and are ubiquitously expressed across a diverse range of life forms, including bacteria, insects, amphibians, and mammals.[6] In light of the escalating challenges posed by antibiotic resistance, AMPs have emerged as promising candidates for the development of effective antibacterial agents.[7] Several cyclic peptide based drugs, though not AMP, such as polymyxins, daptomycin, and vancomycin, have been commercialized for clinical application. These agents are utilized in the treatment of infections caused by antibiotic-resistant Gram-negative bacteria,[8] antibiotic-resistant Gram-positive bacteria,[9] methicillin-resistant *Staphylococcus aureus* (MRSA), and antibiotic-resistant enterococci.[10] AMPs constitute a novel class of antibacterial agents, distinguished by their broad-spectrum efficacy against a wide range of pathogens, including bacteria, fungi, and viruses. A notable safety advantage of AMPs is their biodegradability, as they degrade into amino acids, which are generally non-toxic or biocompatible. Furthermore, AMPs employ multiple, often unique, mechanisms to exert their antibacterial effects. These mechanisms involve the disruption of bacterial membranes, the compromise of cell wall integrity and function, the inhibition of protein synthesis, the impairment of DNA and RNA

School of Pharmacy, Baotou Medical College, Baotou 014060, China. E-mail: 102015128@btmc.edu.cn

† These authors contributed equally.

replication and biosynthesis, as well as the suppression of biofilm formation and the degradation of mature biofilms. This mechanistic diversity markedly reduces the probability of pathogens developing resistance.[11,12] AMPs show considerable promise as innovative anti-biofilm agents, primarily due to their ability to inhibit biofilm formation.[13] However, only a limited number of AMPs,[14] including TEMP-A, CIT-1.1, TP-I-L1,[15] and E-PL,[16] have been documented to exert inhibitory effects against biofilm formation.[16] Moreover, a comprehensive assessment of their therapeutic efficacy and toxicity profiles is necessary. Accordingly, the development of novel anti-biofilm agents featuring potent antibacterial activity, high stability, and low toxicity is urgently required.[17]

American oyster defensin (AOD)[18] is a naturally occurring AMP that exhibits efficacy against both Gram-positive and Gram-negative bacteria. However, its intricate structure—comprising 38 amino acids and three disulfide bridges—renders its chemical synthesis economically costly. Accumulating evidence[19–21] have demonstrated that the synergistic interaction between hydrophobic tryptophan (Trp, W) and cationic arginine (Arg, R), achieved through rational design, can significantly enhance the antibacterial efficacy of peptides. Seo *et al.*[22] successfully designed the AOD analog A4 (CRRWGWRRC) by employing homology modeling of AOD to screen for a template region containing a disulfide bond, followed by the incorporation of Arg and Trp residues. A4 exhibited significant antibacterial activity, with minimum inhibitory concentrations (MIC) ranging from 2.2 to 29.5 μg mL^{-1}. Notably, the MIC against *E. coli* and *B. subtilis* were 2.2 μg mL^{-1} and 2.5 μg mL^{-1}, respectively. Seo *et al.* suggested that A4 exerts its antibacterial effect by binding to DNA or interfering with DNA amplification. Zhao[23] demonstrated that A3, a derivative peptide of AOD, functions through a mechanism that inhibits bacterial biofilm formation. As A4 is also an analogue of AOD, it likely inhibits bacterial biofilm formation *via* a comparable mechanism, thus representing a promising candidate for the development of new anti-biofilm agents.

To develop novel anti-biofilm agents with superior antibacterial activity and enhanced stability, we employed tuning amino acid configuration and substituting disulfide bonds strategy to optimize A4. Specifically, we substituted the L-amino acids in A4 with D-amino acids or replaced the disulfide bonds with a triazole ring to achieve a protease-resistant structure. Among the four analogs evaluated, D-A4 is the best anti-biofilm agent, which displayed equivalent antibacterial potency relative to parent peptide A4 against *Staphylococcus aureus*, *Bacillus subtilis*, *Klebsiella pneumoniae*, *Escherichia coli*, and *Pseudomonas aeruginosa*. Notably, D-A4 achieved a 2-fold reduction in MIC compared with A4 against *Salmonella Paratyphi B* and *Salmonella enterica*. Furthermore, D-A4 exhibited markedly enhanced stability upon exposure to proteolytic enzymes and serum environments. Even at a concentration of 250 μg mL^{-1} (~2–>100 fold higher than MIC), D-A4 maintained low cytotoxicity against normal cells, highlighting its favorable safety profile for potential therapeutic applications. In summary, this study successfully identified D-A4 as a highly active and stable anti-biofilm agent. Importantly, this research not only introduces a novel potential therapeutic agent for combating biofilm-associated chronic infections but also provides a robust theoretical foundation for the development of next-generation anti-biofilm therapeutics.

2 Materials and methods

2.1 Materials

FD-1-50 vacuum freeze dryer, Beijing Boyikang Experimental Instrument Co., Ltd JY2003 Electronic Balance, Shanghai Sunny Hengping Instrument Co., Ltd CHA-S Constant Temperature Shaker, Changzhou Guohua Electric Appliance Co., Ltd Vortex Mixer, Haimen Qilin Bell Instrument Manufacturing Co., Ltd L500-A Centrifuge, Shanghai Xiangyi Centrifuge Instrument Co., Ltd Microplate Reader, Thermo SCIENTIFIC. Shimadzu High-Performance Liquid Chromatography LC-20, Shimadzu Corporation, Japan. Thermo Ultimate 3000+ Preparative/Analytical Chromatograph, Thermo SCIENTIFIC. Chromatography Columns. Welch XB-C18 Column (4.6 × 250 mm, 5 μm), Welch Materials, Inc. (China). Hypersil GOLD™ Preparative Column (10 × 250 mm, 5 μm), Welch Materials, Inc. (China). SHI-3 Circulating Water Vacuum Pump, Shanghai Yarong Biochemical Instrument Factory. Reagents: Rink Amide AM Resin (substitution degree: 0.31 mmol g^{-1}), Tianjin Hecheng Technology Co., Ltd. Fmoc-protected amino acids for target peptide synthesis, including Fmoc-Cys(Trt)-OH, Fmoc-Arg(Pbf)-OH, Fmoc-Trp(Boc)-OH, Fmoc-Gly-OH, *etc.*, purchased from GL Biochem (Shanghai) Ltd. Coupling reagents: 6-chloro-1-hydroxybenzotriazole tetramethyluronium hexafluorophosphate (HCTU) and 2-(7-azabenzotriazol-1-yl)-*N*,*N*,*N*′,*N*′-tetramethyluronium hexafluorophosphate (HATU), purchased from GL Biochem (Shanghai) Ltd. *N*,*N*-diisopropylethylamine (DIEA), dimethyl sulfoxide (DMSO), triisopropylsilane (TIPS), sodium ascorbate, reduced glutathione (GSH), *etc.*, purchased from Aladdin Reagent (Shanghai) Co., Ltd. Anhydrous copper sulfate (analytical grade), trifluoroacetic acid (HPLC grade), trifluoroacetic acid (analytical grade), *N*,*N*-dimethylformamide (DMF), 4-methylpiperidine, *etc.*, purchased from Shanghai Titan Scientific Co., Ltd. DMEM Medium, purchased from Servicebio Technology Co., Ltd. Dichloromethane (DCM), Anhui Tiandi High Purity Solvent Co., Ltd. , Coolaber. Acetonitrile (HPLC grade), J. T. Baker. Methyl *tert*-butyl ether, Beijing Stone Technology Co., Ltd.

2.2 Design and synthesis of A4 analogs

To address the protease susceptibility of A4, the amino acid configuration replacement strategy and substituting disulfide bonds strategy was employed. In amino acid configuration replacement strategy, the natural L-amino acids in A4 were replaced with D-amino acids to yield D-A4. For substituting disulfide bonds strategy, a more robust triazole moiety was utilized to replace the disulfide linkage, resulting in the formation of A4-T1, A4-T2 and A4-T3. Specifically, the cysteine residue at the C-terminus of the A4 was replaced with L-propargylglycine. Simultaneously, the cysteine residue at the *N*-terminus was substituted with a series of azido-functionalized

amino acids, namely, (2)-2-amino-4-azidobutanoic acid, (2*S*)-2-amino-5-azidopentanoic acid, and (2*S*)-2-amino-6-azidohexanoic acid. Subsequently, the azido groups from these *N*-terminal residues and the alkyne group from the C-terminal L-propargylglycine underwent a copper-catalyzed click reaction to form a stable triazole moiety.

Linear D-A4, A4-T1, A4-T2, and A4-T3 were synthesized using Fmoc (9-fluorenylmethoxycarbonyl)-based solid-phase peptide synthesis. Rink amide AM resin (0.31 mmol g^{-1}) was used as the solid support. A total of 300 mg of resin was weighed into a peptide synthesis vessel. Deprotection was carried out using 25% tetramethylpiperidine at 32 °C for 10 min, repeated twice. For amino acid coupling, each coupling reaction was performed twice to ensure complete incorporation, with reaction conditions of 32 °C for 45 min. The amino acids were sequentially assembled onto the resin following the above coupling strategy. After the assembly of all amino acids and removal of the final Fmoc protecting group, 10 mL of cleavage reagent (trifluoroacetic acid (TFA): triisopropylsilane (TIPS) : H_2O = 9.5 : 0.25 : 0.25, v/v/v) was added, and the mixture was incubated at 32 °C for 3 h. After the cleavage reaction, the collected cleavage solution was concentrated under a stream of nitrogen, and ice-cold methyl *tert*-butyl ether was added to precipitate the peptide. The mixture was centrifuged, and the supernatant was discarded. This washing process was repeated twice to obtain the crude linear peptide as a solid.

2.3 Oxidative folding of linear D-A4

The crude linear D-A4 was oxidized, utilizing dimethyl sulfoxide (DMSO) as the oxidizing agent. Specifically, 3 mg of crude linear D-A4 was accurately weighed and transferred into a 5 mL centrifuge tube. Subsequently, 900 μL of phosphate-buffered saline (PBS, pH 7.4) was added to the centrifuge tube, followed by the addition of 100 μL of DMSO. The oxidation reaction occurred at room temperature. The progress of the reaction was monitored *via* reverse-phase high-performance liquid chromatography (RP-HPLC). The resultant D-A4 was subsequently isolated and purified using RP-HPLC, employing a mobile phase consisting of water with 0.1% trifluoroacetic acid (TFA) as phase A and acetonitrile with 0.1% TFA as phase B, with a gradient elution from 30% to 70% phase B. The purified D-A4 solution was pre-frozen in liquid nitrogen and subsequently lyophilized. The molecular mass of D-A4 was confirmed through electrospray ionization mass spectrometry (ESI-MS).

2.4 Click chemistry reactions of linear A4-T1, A4-T2, and A4-T3

The click chemistry reaction[24] was performed using $CuSO_4$ as catalyst. Initially, 3 mg of the linear crude peptide was dissolved in 1 mL of deionized water. In other 2 mL centrifuge tube, 8 mg of $CuSO_4$ and 25 mg of sodium ascorbate ($C_6H_7O_6Na$) were dissolved in 2 mL of deionized water. Subsequently, 100 μL of this prepared solution was promptly added to the peptide solution. The reaction mixture was stirred and allowed to proceed at room temperature, with its progress monitored *via* RP-HPLC. The resulting peptide was isolated and purified using RP-HPLC, employing a mobile phase consisting of water with 0.1% trifluoroacetic acid (TFA) as phase A and acetonitrile with 0.1% TFA as phase B, with a gradient elution from 30% to 70% phase B. The purified peptide was obtained following lyophilization. Finally, the molecular mass of A4-T1, A4-T2, and A4-T3 were confirmed by ESI-MS.

2.5 Circular dichroism (CD) spectroscopy

The compounds D-A4, A4-T1, A4-T2, and A4-T3 were dissolved in PBS containing 10% (v/v) trifluoroethanol (TFE) to prepare peptide solutions at a concentration of 1 mg mL^{-1}. Each solution was subsequently placed in a quartz cuvette with a path length of 1 mm and analyzed using a J-1500 circular dichroism spectrophotometer. The CD spectra were recorded with a scanning bandwidth of 1 nm, covering a wavelength range from 170 nm to 300 nm, at a scanning speed of 200 nm min^{-1}.

2.6 Antibacterial activity of A4 analogs

2.6.1 Agar well diffusion assay. The antibacterial activity of D-A4, A4-T1, A4-T2, and A4-T3 were qualitatively evaluated using the agar well diffusion method.[25] A bacterial suspension was prepared from cultures in the logarithmic growth phase, achieving a concentration of 1×10^8 CFU mL^{-1}. Nutrient agar plates incorporating 5% of the bacterial suspension were prepared. Uniform wells were created in the agar using sterilized 3 mm punches. The peptide solutions were prepared in PBS at a concentration of 1000 μg mL^{-1}. Subsequently, 10 μL of each peptide solution at varying concentrations was introduced into the respective wells, with PBS as the negative control. Each assay was performed in triplicate. The plates were incubated at 37 °C for 24 hours, then they were examined for the presence of inhibition zones.

2.6.2 Broth microdilution assays. Bacterial cultures were grown in nutrient broth medium, and cells in the logarithmic growth phase were collected to prepare a suspension with a concentration of 1×10^6 CFU mL^{-1}. The peptide solutions were prepared in PBS to a concentration of 1000 μg mL^{-1}. MIC was determined using a two-fold serial dilution method.[26] Each concentration was evaluated in triplicate. A row containing solely the bacterial suspension without any compound functioned as the positive control, whereas a row containing only the medium served as the negative control. The plate was then incubated at 37 °C for 18–24 hours. Bacterial growth was assessed visually, and optical density (OD) was measured at 600 nm using a microplate reader.

2.7 Hemolytic activity test of A4 peptide analogs

2.7.1 Hemolysis assay using blood agar plate. The qualitative hemolytic activity of the analogs was assessed using Columbia blood agar plates. A peptide solution was prepared at a concentration of 1000 μg mL^{-1}, with 0.1% Triton X-100 as the positive control and PBS as the negative control. Wells were created in the blood agar plates using the 3 mm punch, and then 10 μL of each solution was added to the respective wells. The plates were then incubated overnight at 37 °C and examined for the presence of hemolysis.

2.7.2 Hemolysis assay using erythrocytes. Quantitative hemolytic activity assays were performed for D-A4 and A4-T1, A4-T2, A4-T3. Blood samples were collected from the mice by orbital blood sampling and transferred into centrifuge tubes containing 2 mg mL^{-1} sodium heparin. The samples were centrifuged at 3000 rpm, the supernatant was discarded, and the red blood cells were isolated. The peptide was dissolved in physiological saline to prepare solution with a concentration of 0.9 to 1000 μg mL^{-1}. Subsequently, 4 μL of the suspension was combined with 200 μL of each peptide solution in a 0.2 mL centrifuge tube. Physiological saline and 0.1% Triton X-100 were used as negative and positive controls, respectively. The mixtures were incubated at 37 °C for 1 hour, followed by centrifugation at 3000 rpm for 5 minutes. The supernatant was transferred to a 96-well plate, and its absorbance at 540 nm was measured using a microplate reader. All experiments were conducted in triplicate. The percentage of hemolysis was calculated using a specified formula.[27]

$$\text{Hemolysis rate (\%)} = (A_{\text{experimental group}} - A_{\text{blank group}})/(A_{\text{positive group}} - A_{\text{blank group}}) \times 100\%$$

2.8 Antibacterial mechanism of A4 analogs

2.8.1 Effect on membrane permeability of *E. coli* ATCC 25922. *E. coli ATCC 25922* was suspended in LB medium and subjected to centrifugation at 4500 rpm for 5 minutes at 4 °C. The resulting bacterial pellet was washed twice with PBS and subsequently resuspended in PBS. The bacterial suspension was then treated with A4, D-A4 and A4-T3 at concentrations of 1 × MIC and 2 × MIC, followed by incubation at 37 °C for 30 minutes. Ethylenediaminetetraacetic acid disodium salt(EDTA) was used as the positive control. After the supernatant was discarded, the cells were resuspended in PBS containing 10 μg mL^{-1} of crystal violet. The bacterial suspension was incubated at 37 °C for 10 minutes and then centrifuged at 13 000 rpm for 15 minutes. The optical density of the supernatant was measured at 590 nm using a UV spectrophotometer, with the OD value of PBS containing 10 μg mL^{-1} of crystal violet designated as 100%. The percentage of crystal violet uptake was calculated using the following formula.[28]

$$\text{Crystal violet uptake (\%)} = (\text{OD}_{590\text{nm}}\ \text{sample}/\text{OD}_{590\text{nm}}\ \text{crystal violet control}) \times 100\%$$

2.8.2 Biofilm inhibition assay. Cultures of *E. coli ATCC 25922*, grown to the logarithmic phase, were used to prepare bacterial suspensions. A 100 μL aliquot of the bacterial suspension was dispensed into each well of a 96-well plate. Subsequently, A4, D-A4 or A4-T3 was added at concentrations of 1/2 × MIC, 1 × MIC, 2 × MIC, 4 × MIC, and 8 × MIC. The plate was incubated at 37 °C for 20 hours in a constant-temperature incubator. After incubation, the plate was centrifuged at 3000 rpm for 5 minutes. The supernatant was carefully removed using a pipette, and each well was washed three times with 100 μL of PBS. To fix the remaining biofilm, 100 μL of absolute methanol was added to each well and allowed to stand for 15 minutes before being discarded. Subsequently, 100 μL of 0.1% crystal violet staining solution was added to each well and left to stain for 30 minutes. The staining solution was then removed, and the wells were rinsed with PBS until the PBS appeared colorless. To dissolve the biofilm, 200 μL of 95% ethanol was added to each well, followed by incubation at 37 °C for 30 minutes. Finally, the plate was placed in a microplate reader to measure the absorbance at 595 nm. Each experiment was repeated three times.

2.9 Stability of A4 analogs

2.9.1 Protease stability. For the trypsin degradation assay, trypsin was used at a concentration of 1.5 ng mL^{-1}, while either D-A4 or A4-T3 was employed at a concentration of 1 mg mL; both trypsin or peptides were dissolved in PBS (pH 7.4) prior to the assay. Specifically, 900 μL of the trypsin solution was dispensed into a 1.5 mL centrifuge tube. Subsequently, 100 μL of each peptide solution was added to the tube containing the trypsin. The degradation reaction was maintained at 37 °C. During the assay, 100 μL aliquots of the reaction mixture were collected at predetermined intervals: 0, 1, 2, 4, 8, and 10 minutes. Each aliquot was promptly quenched by the addition of 30 μL of 1 M HCl. The entire reaction process was monitored using RP-HPLC.

2.9.2 Serum stability. The stability of D-A4 and A4-T3 under serum conditions was assessed. The MIC of peptides against *E. coli ATCC 25922* were evaluated in environments with serum concentrations of 50%, 25%, and 0%. The MIC were determined using the microbroth dilution technique as outlined in Section 2.6.2, with bacterial growth quantified by measuring absorbance at 600 nm.

2.10 Cell counting Kit-8(CCK-8)

Mouse peritoneal macrophage RAW 264.7 cells were diluted to a concentration of 1.5×10^4 cells mL^{-1}, and 100 μL of this cell suspension was uniformly distributed into each well of a 96-well plate. To mitigate edge effects, 200 μL of PBS was added to each well in the outermost row of the plate. The plate was subsequently incubated at 37 °C with 5% CO_2 overnight. Following incubation, the culture medium was replaced with 100 μL of fresh medium containing either D-A4 or A4-T3 at concentrations of 500, 250, 125, and 62.5 μg mL^{-1}, which were added to the designated wells. After 24 hours of exposure to the compounds, the medium was carefully aspirated. Subsequently, 100 μL of medium containing 10% CCK-8 reagent was added to each well, and the plate was incubated in the dark at 37 °C with 5% CO_2. Absorbance measurements were taken every 30 minutes using a full-wavelength microplate reader, and the density at 450 nm (OD_{450nm}) was recorded. Data were plotted using GraphPad Prism. The experimental setup included the following groups: blank group (medium only), control group (cells + medium) and experimental group (cells + medium + drug).

Cell viability (%) = (OD_{450nm} experimental well − OD_{450nm} blank well)/(OD_{450nm} control well − OD_{450nm} blank well) × 100%

2.11 Time-kill curve

E. coli ATCC 25922 was cultured to the logarithmic phase. The culture was diluted with physiological saline to a turbidity of 0.5 McFarland standard, followed by a 150-fold dilution with LB medium to achieve a final bacterial suspension density of 1 × 10^6 CFU mL^{-1}. The physiological saline group served as the negative control. D-A4 and A4-T3, at concentrations of 1 × MIC and 4 × MIC, were separately mixed with the bacterial suspension in sterile microcentrifuge tubes. The tubes were then incubated at 37 °C in a constant-temperature incubator. 10 μL of samples were collected at 0 h, 3 h, 6 h, 9 h, 12 h, and 24 h, and then samples were serially diluted. A 5 μL aliquot of each diluted sample was spotted onto nutrient agar plates, spread evenly, and the plates were incubated at 37 °C for 22 hours. After incubation, the colonies on each plate were counted, and the CFU corresponding to each compound concentration at each time point was calculated and converted to $\log_{10}$ CFU mL^{-1}. A time-kill curve was plotted with time on the *x*-axis and $\log_{10}$ CFU mL^{-1} on the *y*-axis. The experiment was performed in triplicate.

2.12 Scanning electron microscopy (SEM)

Bacterial cultures in the logarithmic growth phase were harvested to prepare a 5 mL suspension of *E. coli ATCC 25922* at a concentration of 1 × 10^8 CFU mL^{-1}. The bacterial cells were pelleted by centrifugation at 5000 rpm for 8 minutes and subsequently treated with D-A4 and A4-T3 at a concentration of 2 × MIC. As a blank control, an equivalent volume of PBS was used to treat the bacteria. Following thorough mixing of the agents with the bacterial suspension, the mixture was incubated at 37 °C for 2 hours. After incubation, the samples underwent another centrifugation at 5000 rpm for 8 minutes, and the supernatant was carefully decanted. The bacterial pellets were fixed overnight at 4 °C using 2.5% glutaraldehyde. The fixed samples were then subjected to gradient dehydration using ethanol concentrations of 50%, 70%, 90%, 95%, and 100%, with each step lasting 10 minutes. After dehydration, the samples were dried, mounted on conductive adhesive, and sputter-coated with gold. Finally, the specimens were examined using SEM.

3 Results

3.1 Synthesis of peptides

3.1.1 Synthesis of D-A4. In this study, a solid-phase peptide synthesis approach utilizing Fmoc protection[29] was employed, resulting in the successful synthesis of linear D-A4, as depicted in Fig. 1. The unpurified linear D-A4 was subjected to oxidation using DMSO as oxidant, and the progress of the oxidation was monitored *via* RP-HPLC. The corresponding results are illustrated in Fig. 2. Upon addition of DMSO, the peak intensity of linear D-A4 decreased, accompanied by an increase in the peak intensity of D-A4. The oxidation was complete within 120 minutes. Following the completion of the reaction, the product was isolated and purified using RP-HPLC, successfully yielding D-A4. The successful synthesis of D-A4 was confirmed by ESI-MS analysis, as the measured molecular weight was consistent with the theoretical value.

3.1.2 Synthesis of A4-T1, A4-T2 and A4-T3. To improve the stability of A4, the disulfide bonds in A4 were replaced with a stable triazole moiety, affording A4-T1, A4-T2, and A4-T3 (Fig. 3 and 4). The linear A4-T1, A4-T2, and A4-T3 was prepared by Fmoc-SPPS. The click reactions of unpurified linear A4-T1, A4-T2, and A4-T3 were catalyzed by $CuSO_4$, with the reaction progress monitored through RP-HPLC. As shown in

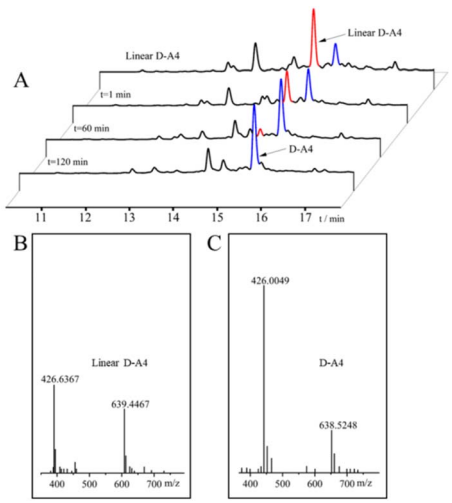

Fig. 2 (A) Oxidation of linear D-A4; (B) the ESI-MS of linear D-A4; (C) the ESI-MS of D-A4.

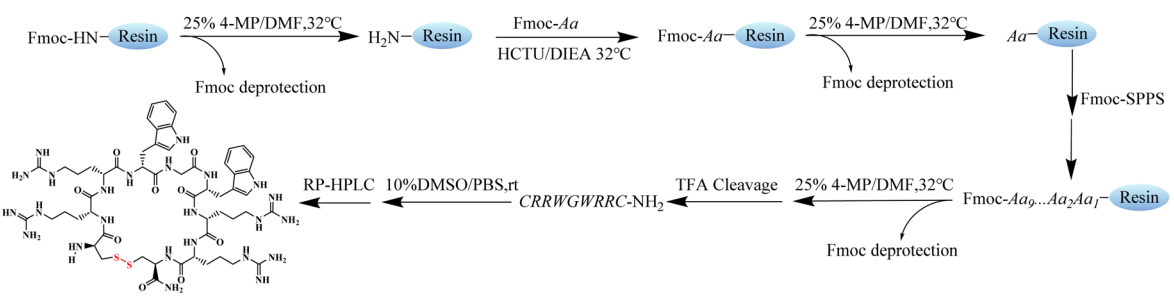

Fig. 1 The synthetic route of D-A4.

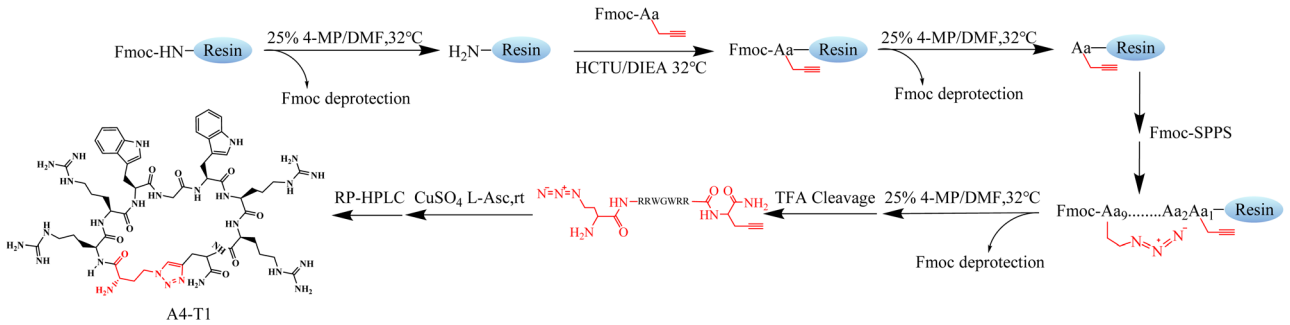

Fig. 3 The synthetic route of A4-T1.

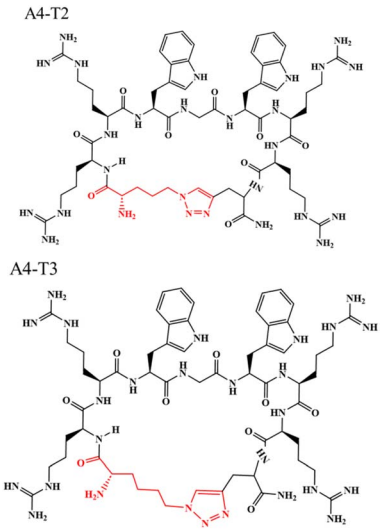

Fig. 4 The structures of A4-T2 and A4-T3.

Fig. 5–7, the peaks of the linear peptides (in red) gradually diminished, while new peaks (corresponding to the cyclic products, in blue) appeared with shorter retention times The click reactions of linear A4-T1, A4-T2, and A4-T3 were completed within 45 minutes. The products were subsequently isolated and purified using RP-HPLC, yielding A4-T1, A4-T2, and A4-T3. The successful synthesis of A4-T1, A4-T2, and A4-T3 was confirmed by ESI-MS data of linear peptides and cyclic peptides.

3.2 The secondary structure of A4 analogs

To determine the secondary structures of D-A4, A4-T1, A4-T2, and A4-T3, the peptides were dissolved at 1 mg mL^{-1} in PBS

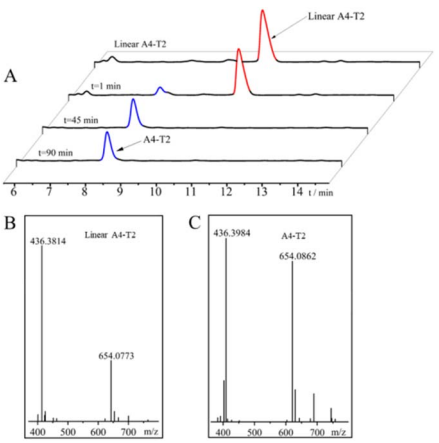

Fig. 6 (A) The click reaction of linear A4-T2; (B) the ESI-MS of linear A4-T2; (C) the ESI-MS spectrum of A4-T2.

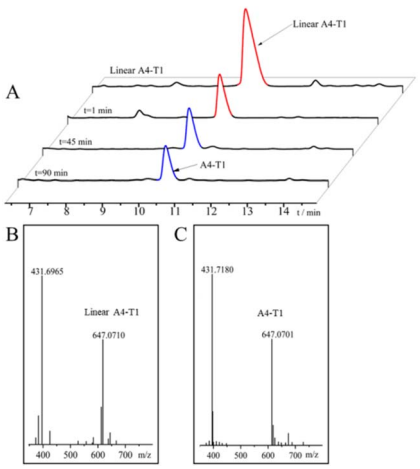

Fig. 5 (A) The click reaction of linear A4-T1; (B) the ESI-MS of linear A4-T1; (C) the ESI-MS spectrum of A4-T1.

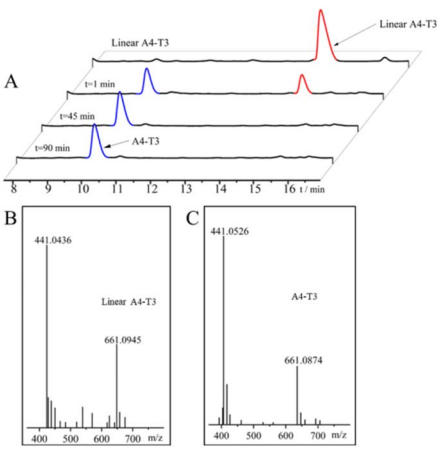

Fig. 7 (A) The click reaction of linear A4-T3; (B) the ESI-MS of linear A4-T3; (C) the ESI-MS spectrum of A4-T3.

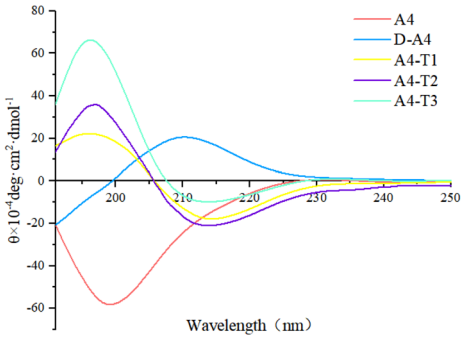

Fig. 8 CD spectra of A4 analogs.

(pH 7.4) containing 10% TFE, and their secondary structures were analyzed by CD spectra. As shown in Fig. 8, A4 exhibited a negative peak around 200 nm, indicative of a disordered structure. In contrast, D-A4 exhibited a positive peak around 210 nm. The CD curve of D-A4 was opposite to the curve of A4, but not a perfect mirror image. This may be due to certain conformational differences between them. This spectral feature is characteristic of peptides with the D-configuration, demonstrating that D-A4 also adopts a disordered structure but with inverted chirality. Collectively, these results confirmed the successful synthesis of D-A4. The CD spectra of A4-T1, A4-T2, and A4-T3 exhibited a positive peak near 198 nm and a negative peak near 215 nm, a characteristic feature of a β-sheet structure. These CD results indicate that after replacing the disulfide bonds, the structure of the A4 analogs has undergone a significant change, transforming from the original disordered structure to a β-sheet structure.

3.3 Antibacterial activity of A4 analogs

3.3.1 Agar well diffusion assay. The antibacterial activity of the A4 analogs was qualitatively assessed using the agar well diffusion method. The analogs were tested against *B. subtilis*, *S. aureus*, *B. cereus*, *E. coli*, *S. Paratyphi B*, and *P. aeruginosa* at a concentration of 1 mg mL^{-1}. The size of the inhibition zone on the plate is shown in Fig. 9. D-A4, A4-T1, A4-T2, and A4-T3 all produced inhibition zones against Gram-positive (G^+) and Gram-negative (G^-) bacteria, demonstrating broad-spectrum antibacterial activity. Specifically, all four Analogs formed distinct inhibition zones against Gram-positive bacteria (*B. subtilis*, *S. aureus and B. cereus*) and Gram-negative bacteria (*E. coli*, *S. Paratyphi B*, and *P. aeruginosa*) at a concentration of 1 mg mL^{-1}. Comparison of the inhibition zones indicated that D-A4 possessed the most potent activity among all Analogs. Notably, D-A4 exhibited a markedly larger inhibition zone relative to A4, highlighting its superior antibacterial activity. The antibacterial effect of A4-T3 against *B. subtilis*, *S. aureus*, *B. cereus*, and *P. aeruginosa* was comparable to that of A4, whereas A4-T1 and A4-T2 displayed diminished antibacterial activity relative to A4 against all tested bacterial strains.

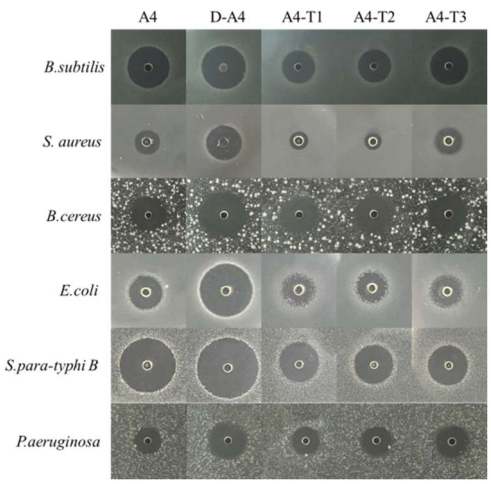

Fig. 9 Qualitative antibacterial activity of A4 analogs against G^+ and G^-.

3.3.2 Broth microdilution assay. The MICs of D-A4, A4-T1, A4-T2, and A4-T3 were determined against a panel of bacterial strains using the broth microdilution method. The tested strains included *S. aureus*,*S. aureus ATCC 25923*, *B. subtilis CMCC 63501*, *K. pneumoniae*, *E. coli ATCC 25922*, *P. aeruginosa ATCC 27853*, *S. enterica*, and *S. paratyphi B.* The MIC values of all tested peptides are presented in Table 1. D-A4, A4-T1, A4-T2, and A4-T3 exhibited inhibitory activity against both Gram-positive and Gram-negative bacteria. Specifically, for the three Gram-positive bacterial strains (*S. aureus*, *S. aureus ATCC 25923*, and *B. subtilis CMCC 63501*) D-A4 exhibited antibacterial activity comparable to that of A4, whereas the triazole-substituted peptides displayed a 2-4-fold reduction in antibacterial activity. Among the triazole-substituted peptides, A4-T3 displayed the most potent antibacterial activity. For the three Gram-negative bacterial strains (*K. pneumoniae*, *E. coli ATCC 25922*, *P. aeruginosa ATCC 27853*) D-A4 exhibited the same antibacterial activity as A4, with the lowest MIC value of 1.9 μg mL^{-1}. Notably, for *K. pneumoniae*, the triazole-substituted peptides exhibited lower MICs than both A4 and D-A4. Furthermore, for *S. enterica* and *S. Paratyphi B*, the antibacterial activity of D-A4 was twice that of A4. The findings from the quantitative experiments corroborate the results obtained in the qualitative assays, thereby validating the experimental accuracy. Overall, these data indicated that D-A4 possesses superior antibacterial activity compared to A4 and the triazole-substituted peptides. Among the triazole-substituted peptides, A4-T3 was demonstrated to have the most pronounced antibacterial activity. This observation may be attributed to the different ring sizes of the triazole-substituted peptides, resulting in their different antibacterial potency. Nevertheless, the antibacterial activity of the triazole-substituted peptides is marginally lower than that of A4. This discrepancy may be linked to the structural transition of the peptide from a disordered conformation to a β-sheet configuration. It is posited that the disordered structure plays a crucial role in mediating the antibacterial effects of A4.

3.4 Hemolytic activity of A4 analogs

3.4.1 Qualitative hemolytic activity of A4 analogs. The hemolytic activity of A4 analogs was qualitatively assessed using

Table 1 Minimum inhibitory concentration of A4 analogs

		Minimum inhibitory concentration (μg mL^{-1})					
Microbe	Gram stain	A4	D-A4	A4-T1	A4-T2	A4-T3	Doxycycline[30]
S. aureus	+	31.2	31.2	125.0	125.0	125.0	0.45
S. aureus ATCC 25923	+	31.2	31.2	125.0	62.5	62.5	0.224
B.subtilis CMCC 63501	+	7.8	7.8	31.2	31.2	15.6	N.T.[a]
K. pneumoniae	−	125.0	125.0	62.5	62.5	62.5	2
E.coli ATCC 25922	−	1.9	1.9	3.9	3.9	3.9	15.63
P.aeruginosa ATCC 27853	−	31.2	31.2	62.5	62.5	62.5	N.T.[a]
S.enterica	−	125.0	62.5	125.0	125.0	62.5	15.63
S.paratyphi B	−	3.9	1.9	7.8	7.8	7.8	N.T.[a]

[a] N.T., not tested.

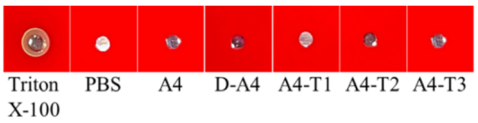

Fig. 10 Qualitative hemolytic activity of A4 analogs on blood agar plates.

the Columbia blood agar well diffusion method. Blood agar plates were incubated overnight with A4 analogs at a concentration of 1 mg mL^{-1}, using 0.1% Triton X-100 as a positive control and PBS (pH 7.4) as a negative control. The data are shown in Fig. 10. The positive control well exhibited a distinct yellow hemolytic ring, signifying complete hemolysis. In contrast, no yellow hemolytic rings were observed around the negative control wells, indicating the absence of hemolysis. Similarly, the wells containing the A4 analogs showed the same appearance as the negative control, with no visible hemolytic rings. These results indicated that the A4 analogs exhibited no detectable hemolytic activity even at the high concentration of 1 mg mL^{-1}.

3.4.2 Quantitative hemolytic activity of A4 analogs. The quantitative hemolytic activity of A4 analogs was determined using mouse erythrocytes. The data are shown in Fig. 11. The positive control was treated with 0.1% Triton X-100, exhibiting complete hemolysis (100%), whereas the negative control was treated with PBS at pH 7.4, exhibiting no hemolysis. Even if the concentration rose to 1000 μg mL^{-1}, the hemolysis rates of all A4 analogs remained below 5%, indicating excellent hemocompatibility. Notably, at the highest concentration of 1000 μg mL^{-1}, the hemolysis rates of D-A4, A4-T1, T2, and T3 were minimal and lower than that of A4, further confirming their safety even at high concentrations. These findings provide critical evidence supporting the safety of D-A4, A4-T1, T2, and T3 as potential therapeutic agents for systemic administration *via* injection for treatment against *E. coli*, *B. subtilis*, *S. aureus*, *P. aeruginosa* and *S. paratyphi B*.

3.5 Antibacterial mechanism of D-A4 and A4-T3

3.5.1 Membrane permeabilization of D-A4 and A4-T3 in *E. coli ATCC 25922*. Based on their superior antibacterial activity, D-A4 and A4-T3 were selected for further evaluation of their antibacterial mechanism. To investigate the effect of D-A4 and A4-T3 on membrane permeabilization, a crystal violet uptake assay was performed using PBS (pH 7.4) and 0.25 M EDTA as negative and positive control, respectively. The data of this assay are presented in Fig. 12. Crystal violet uptake rate of EDTA treatment was 62.5%, confirming the assay's validity for detecting changes in membrane permeabilization. After treatment with A4, D-A4, or A4-T3 at 1 × MIC or 2 × MIC, *E. coli ATCC 25922* showed similar levels of permeabilization compared to the negative control, suggesting the increase in concentration could not affect the membrane permeabilization.

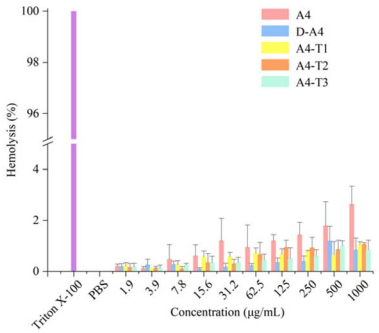

Fig. 11 Quantitative hemolytic activity of A4 analogs.

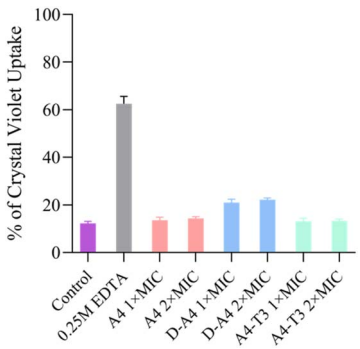

Fig. 12 Effect of D-A4 and A4-T3 on the membrane permeabilization of *E. coli ATCC 25922*.

These results indicate that D-A4 and A4-T3 does not directly act on the bacterial membrane to induce alterations in membrane permeability. This finding is consistent with the results reported by Seo,[6] who demonstrated that the antibacterial effect of A4 was not mediated by membrane disruption.

3.5.2 Inhibition of bacterial biofilm activity by D-A4 and A4-T3. To further explore the anti-biofilm potential of D-A4 and A4-T3, their ability to inhibit biofilm formation of *E. coli ATCC 25922* was evaluated using the crystal violet staining method, with concentrations ranging from 1/2 × MIC to 8 × MIC. As shown in Fig. 13, A4, D-A4, and A4-T3 effectively inhibited biofilm formation in all tested concentrations, and the biofilm inhibition rate increased in a concentration-dependent manner. At concentrations ranging from 1/2 × MIC to 1 × MIC, A4-T3 exhibited a weaker inhibitory effect than D-A4, which is consistent with their respective antibacterial potencies. These findings reveal a positive correlation between antibacterial efficacy and anti-biofilm capacity, with stronger biofilm inhibition corresponding to enhanced antibacterial activity. At concentrations ranging from 2 × MIC to 8 × MIC, A4, D-A4, and A4-T3 exhibited comparable biofilm inhibition activities. Remarkably, indicate retained potent anti-biofilm activity even at the sub-MIC concentration of 1/2 × MIC, with approximately 80% inhibition achieved. These results indicate that one of the mechanisms by which A4, D-A4, and A4-T3 exert their antibacterial effects is direct inhibition of biofilm formation, highlighting them as efficient anti-biofilm agents for combating the growing threat of antibiotic resistance.

3.6 Stability of D-A4 and A4-T3

3.6.1 High stability of D-A4 in protease environment. Based on their superior activity, D-A4 and A4-T3 were selected for further evaluation of their protease stability. The peptides (1 mg mL^{-1}) were incubated with trypsin (1.5 ng mL^{-1}). The entire reaction process was monitored using RP-HPLC. As shown in Fig. 14, A4 and A4-T3 were completely degraded within 15 min, indicating that peptides composed of L-amino acids are highly susceptible to proteolytic degradation. The half-lives of A4 and A4-T3 were 3.4 minutes and 2.6 minutes respectively. In contrast, no significant degradation of D-A4 was observed even after 24 hours. These results demonstrate that D-A4 possesses high protease stability, which is attributable to its D-amino acid composition that confers resistance to protease recognition and cleavage.

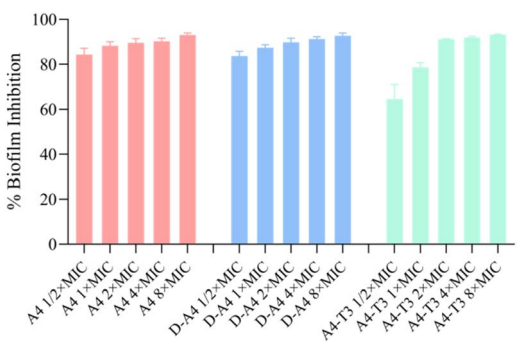

Fig. 13 Biofilm inhibition of D-A4 and A4-T3.

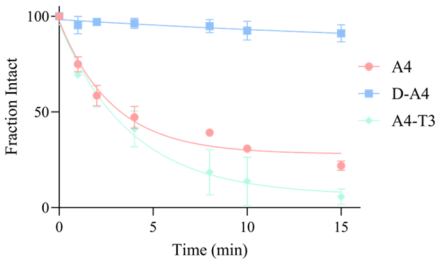

Fig. 14 Trypsin degradation profiles of D-A4 and A4-T3.

Table 2 MIC of antibacterial peptides at different serum concentrations (μg mL^{-1})

	Minimum inhibitory concentration (μg mL^{-1})		
Serum content	A4	D-A4	A4-T3
50%	6.3	1.6	6.3
25%	3.1	1.6	3.1
0	1.6	1.6	3.1

3.6.2 Serum stability of D-A4. The serum stability of D-A4 and A4-T3 was assessed by measuring their MICs against *E. coli ATCC 25922* in the presence of varying concentrations of fetal bovine serum. The data of the serum stability investigation are presented in Table 2. An increase in fetal bovine serum concentration corresponded with a notable rise in the MIC values for both A4 and A4-T3, indicating a serum concentration-dependent effect. Specifically, at 25% serum concentration, the antibacterial activity of A4 was significantly reduced by approximately 2-fold, whereas at 50% serum concentration, its activity was decreased by approximately 4-fold. In contrast, A4-T3 exhibited a 2-fold reduction in MIC at 50% serum concentration but no significant change at 25% serum concentration, indicating its greater stability than A4 under these conditions. The observed decrease in antibacterial activity of A4 and A4-T3 at the tested serum concentrations is likely attributable to proteolytic instability of the compounds or their binding to plasma proteins. Notably, A4-T3 exhibited greater stability than A4 at 25% and 50% serum concentrations, attributed to its triazole moiety, which conferred increased resistance to serum proteases. In contrast, D-A4 consistently maintains a MIC of 1.9 μg mL^{-1} across various fetal bovine serum concentrations, indicating its superior serum stability. This data suggests that D-A4's antibacterial activity remains unaffected by fluctuations in the tested serum concentration. The incorporation of D-amino acids is primarily responsible for the remarkable stability of D-A4, as it effectively resists proteolytic degradation. Consequently, D-A4 is anticipated to sustain prolonged activity *in vivo*, potentially reducing the required dosage and frequency of administration, and ultimately enhancing therapeutic efficacy and patient compliance. This serum stability has significant implications for the clinical development of D-A4.

3.7 Low cytotoxicity of D-A4

The cytotoxicity of D-A4 and A4-T3 against RAW 264.7 macrophages was quantitatively assessed using the CCK-8 assay. As shown in Fig. 15, both D-A4 and A4-T3 exhibited concentration-dependent cytotoxicity against RAW 264.7 macrophages. Notably, D-A4 maintained relatively low toxicity even at higher concentrations, specifically at 250 μg mL^{-1} (~2–>100 fold higher than MIC), with D-A4 exhibiting higher macrophage viability compared to A4. Furthermore, A4-T3 displayed reduced cytotoxicity relative to both A4 and D-A4 across all tested concentrations, resulting in slightly enhanced cell viability. These observations suggest that D-A4 inflicts minimal damage on host cells while preserving therapeutic efficacy, thereby indicating a favorable safety profile.

3.8 Time-kill curve of D-A4, A4-T3

The bactericidal activity and speed of D-A4 and A4-T3 against *E. coli ATCC 25922* was evaluated using time-kill assays over 30 hours at 1 × MIC and 4 × MIC. Normal saline served as a negative control. The outcomes are depicted in Fig. 16. The PBS-treated *E. coli ATCC 25922* grew rapidly within 0–11 hours, then reaching a plateau. Upon exposure to 1 × MIC of D-A4 and A4-T3, approximately 30% of the bacteria were killed within the first 3 hours, with complete eradication achieved by 9 hours. When the concentration reached to 4 × MIC, the bactericidal effects of D-A4 and A4-T3 were notably expedited, resulting in the elimination of 50% to 60% of the bacteria within 3 hours and total bacterial eradication within 6 hours. The bactericidal kinetics of D-A4 and A4-T3 were comparable to those observed with A4. The results from the time-kill curve analysis suggest that D-A4 and A4-T3 exhibit potent bactericidal activity and speed against *E. coli ATCC 25922*, demonstrating a concentration-dependent bactericidal effect. These findings highlight that the bactericidal activity of D-A4 displays time-dependent dynamics, offering crucial implications for refining drug administration strategies. Given its concentration-dependent efficacy profile, a high-dose, low-frequency dosing paradigm emerges as a favorable strategy to amplify therapeutic outcomes while mitigating potential adverse reactions.[31]

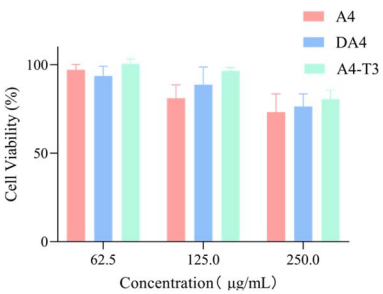

Fig. 15 Cytotoxicity of D-A4 and A4-T3.

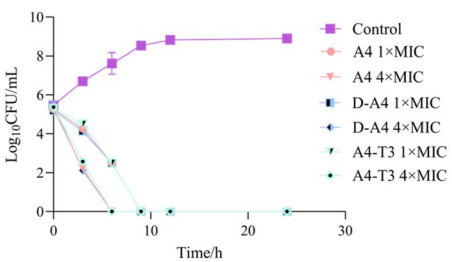

Fig. 16 Time-kill curve of D-A4 and A4-T3 against *E. coli ATCC 25922*.

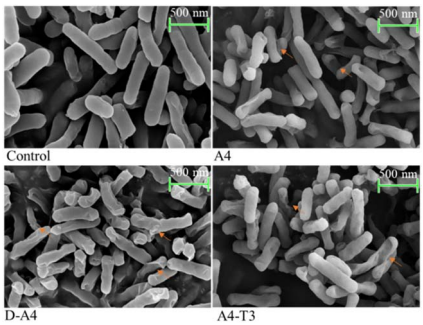

Fig. 17 SEM of D-A4 and A4-T3.

3.9 D-A4 and A4-T3 damage bacterial morphology

The effect of D-A4 and A4-T3 on bacterial morphology was examined by scanning electron microscopy (SEM) after treating *E. coli ATCC 25922* with 4 × MIC of each peptide. In the untreated control group, *E. coli ATCC 25922* displayed a typical rod-shaped morphology with an intact, smooth surface and uniform cell length. No membrane damage, leakage of intracellular contents, or morphological abnormalities were observed. In contrast, treatment with A4, D-A4, and A4-T3 caused severe morphological damage to the bacterial cells, including extensive collapse, rupture, and deformation (Fig. 17). Among the peptide treated *E. coli ATCC 25922*, D-A4 treated *E. coli* exhibited the most severe surface damage. This SEM result is consistent with the superior antibacterial efficacy of D-A4 as demonstrated by the broth microdilution assay, indicating that D-A4 is a highly promising anti-biofilm agent.

4 Conclusions

To address the limitations of A4, specifically its susceptibility to protease degradation and poor stability in serum, four analogs (D-A4, A4-T1, A4-T2, and A4-T3) were successfully synthesized. All four analogs exhibited broad-spectrum antibacterial activity against both Gram-positive and Gram-negative bacteria. D-A4 showed enhanced activity relative to A4, whereas A4-T1, A4-T2, and A4-T3 were generally less active, with A4-T3 being the most potent among them. Hemolysis assays revealed that all four analogs were non-hemolytic (hemolysis <5%) even at 1000 μg mL^{-1}, exhibiting significantly lower hemolytic activity than A4. Mechanistic studies revealed that D-A4 and A4-T3 potently inhibit biofilm formation, positioning them as promising anti-biofilm agents. Stability tests showed that D-A4 exhibited high stability in both proteolytic and serum environments.

Cytotoxicity assays indicated that A4-T3 and D-A4 were less cytotoxic than A4, even at 250 μg mL^{-1} (~2–>100 fold higher than MIC). Time-kill assays demonstrated that the bactericidal activity of D-A4 and A4-T3 was concentration-dependent, with higher concentrations markedly reducing the time to achieve complete killing. SEM analysis revealed that treatment of *E. coli* ATCC-25922 with A4, D-A4, and A4-T3 at 4 × MIC induced noticeable damage to the bacterial surface, indicating that D-A4 can significantly alter bacterial morphology. These findings provide new molecule for drug development and hold promise for improving the treatment of chronic infections.

In conclusion, through rational design and synthesis, this study obtained D-A4 with high activity and stability. It can serve as candidate molecule for novel anti-biofilm agents, providing a promising new strategy to address the global antibiotic resistance crisis, especially biofilm-related infections, and laying a foundation for the future research, development, and optimization of antibacterial drugs.

Ethical statement

All animal procedures were performed in accordance with the Guidelines for Care and Use of Laboratory Animals of Baotou Medical College and approved by the Animal Ethics Committee of Baotou Medical College.

Author contributions

Methodology, conceptualization, data curation, writing original draft, Xin Zhang and Yu Liu. Methodology, data curation, Zhixing Geng. Supervision and review, Ye. Guo. All authors have read and agreed to the published version of the manuscript.

Conflicts of interest

There are no conflicts to declare.

Data availability

The data supporting this article have been included as part of the supplementary information (SI). Supplementary information: structure and reaction curve of A4, mass spectrum data of A4 analogs and HPLC spectra of A4 analogs against trypsin. See DOI: https://doi.org/10.1039/d6ra02550a.

Acknowledgements

This research was funded by the Natural Science Foundation of Inner Mongolia, grant number 2023MS02001, and 2022 Inner Mongolia Autonomous Region "Grassland Talents" Project Youth Innovation and Entrepreneurship Talent Project, grant numbers 2022CYYC1C88, and Science Research Development Foundation of Baotou Medical College, grant number BYJJ-GCJH 202614.

References

1 A. Almatroudi, *Biology*, 2025, **14**(2), 165.
2 Y. Dutt, R. Dhiman, T. Singh, A. Vibhuti, A. Gupta, R. P. Pandey, V. S. Raj, C. M. Chang and A. Priyadarshini, *Antibiotics*, 2022, **11**(7), 930.
3 K. Azeem, S. Fatima, A. Ali, A. Ubaid, F. M. Husain and M. Abid, *Life*, 2025, **15**(1), 49.
4 A. V. Samrot, A. Abubakar Mohamed, E. Faradjeva, L. Si Jie, C. Hooi Sze, A. Arif, T. Chuan Sean, E. Norbert Michael, C. Yeok Mun, N. Xiao Qi, P. Ling Mok and S. S. Kumar, *Medicina*, 2021, **57**(8), 839.
5 J. Zhou, Z. Wang, C. Yang, H. Zhang, M. S. Fareed, Y. He, J. Su, P. Wang, Z. Shen, W. Yan and K. Wang, *Acta Biomater.*, 2022, **151**, 223.
6 N. G. Oliveira Júnior, C. M. Souza, D. F. Buccini, M. H. Cardoso and O. L. Franco, *Nat. Rev. Microbiol.*, 2025, **23**(11), 687.
7 S. Ji, F. An, T. Zhang, M. Lou, J. Guo, K. Liu, Y. Zhu, J. Wu and R. Wu, *Eur. J. Med. Chem.*, 2024, **265**, 116072.
8 Z. Cai, Y. Zhang, Y. Xin, L. Han, B. Xu, M. Du and Y. Zhao, *ACS Infect. Dis.*, 2025, **11**(12), 3394.
9 I. Rezzoug, E. Zamparini, C. Court, A. Mizrahi, L. Dortet and C. Emeraud, *ASM Case Rep.*, 2025, **1**(6), e00106.
10 M. Wang, H. Lv, L. Han, H. Jia, L. Zhang, L. Wang, A. He and Y. Du, *APMIS*, 2025, **133**(9), e70056.
11 M. Rima, M. Rima, Z. Fajloun, J. M. Sabatier, B. Bechinger and T. Naas, *Antibiotics*, 2021, **10**(9), 1095.
12 J. Talapko, T. Meštrović, M. Juzbašić, M. Tomas, S. Erić, L. Horvat Aleksijević, S. Bekić, D. Schwarz, S. Matić, M. Neuberg and I. Škrlec, *Antibiotics*, 2022, **11**(10), 1417.
13 J. Zhang, D. Zhang, Y. Chen, Y. Gong, B. Yuan, Z. Mo, H. Tang, J. Tao and Z. Xu, *Front. Cell. Infect. Microbiol.*, 2025, **14**, 1463551.
14 P. Jorge, D. Grzywacz, W. Kamysz, A. Lourenço and M. O. Pereira, *PLoS One*, 2017, **12**(3), e0174654.
15 S. Wu, Q. Jiang, D. Lu, X. Zhai, J. Duan and B. Hou, *npj Mater. Degrad.*, 2024, **8**(1), 122.
16 D. Pletzer and R. E. Hancock, *J. Bacteriol.*, 2016, **198**, 2572.
17 R. Debroy and S. Ramaiah, *Biofouling*, 2023, **39**(9–10), 928–947.
18 J. K. Seo, J. M. Crawford, K. L. Stone and E. J. Noga, *Biochem. Biophys. Res. Commun.*, 2005, **338**(4), 1998–2004.
19 S. Futaki and I. Nakase, *Acc. Chem. Res.*, 2017, **50**(10), 2449–2456.
20 A. Walrant, A. Bauzá, C. Girardet, I. D. Alves, S. Lecomte, F. Illien, S. Cardon, N. Chaianantakul, M. Pallerla, F. Burlina, A. Frontera and S. Sagan, *Biochim. Biophys. Acta, Biomembr.*, 2020, **1862**(2), 183098.
21 C. H. Yang, Y. C. Chen, S. Y. Peng, A. P. Tsai, T. J. Lee, J. H. Yen and J. W. Liou, *Sci. Rep.*, 2018, **8**(1), 14602.
22 J. K. Seo, D. G. Kim, J. E. Lee, K. S. Park, I. A. Lee, K. Y. Lee, Y. O. Kim and B. H. Nam, *Mar. Drugs*, 2021, **19**(8), 451.
23 J. Zhao, X. Zhang, Y. Liu, Z. Geng, J. Dai and Y. Guo, *RSC Adv.*, 2025, **15**(25), 19954–19965.

24 M. Devi, S. Jaiswal, N. Yaduvanshi, S. Jain, S. Jain, K. Verma, R. Verma, D. Kishore, J. Dwivedi and S. Sharma, *J. Mol. Struct.*, 2023, **1286**, 135571.
25 Y. Wang, B. Cai, D. Ni, Y. Sun, G. Wang and H. Jiang, *J. Nanobiotechnol.*, 2022, **20**(1), 112.
26 H. Deng, Y. Kong, J. Zhu, X. Jiao, Y. Tong, M. Wan, Y. Zhao, S. Lin, Y. Ma and X. Meng, *Curr. Res. Food Sci.*, 2022, **5**, 1559–1569.
27 D. Zhang, S. Cheng, J. Tan, J. Xie, Y. Zhang, S. Chen, H. Du, S. Qian, Y. Qiao, F. Peng and X. Liu, *Bioact. Mater.*, 2022, **17**, 394–405.
28 S. Marito, S. Keshari, S. Traisaeng, D. T. T. My, A. Balasubramaniam, P. Adi, M. F. Hsieh, D. R. Herr and C. M. Huang, *Sci. Rep.*, 2021, **11**(1), 12001.
29 H. Yin, X. Y. Fu, H. Y. Gao, Y. N. Ma, J. F. Yao, S. S. Du, Y. K. Qi and K. W. Wang, *Bioorg. Chem.*, 2023, **138**, 106674.
30 E. Mavrić-Scholze, A. Gusinac, M. Dekić, I. Palić, E. Avdović, D. Simijonović, M. Grujović, K. Marković, V. Dobričić, J. Bošković, Z. Marković and N. Radulović, *Molecules*, 2025, **30**(23), 4606.
31 Z. Yang, S. He, Y. Wei, X. Li, A. Shan and J. Wang, *Phytomedicine*, 2023, **120**, 155070.